Global NEST Journal, Vol 26, No 5, 06173

Improving the energy efficiency and carbon dioxide reduction of a long-haul bus through aerodynamic design optimization

S. Sunil and K. Arunachalam
Department of Automobile Engineering, MIT Campus, Anna University, Chennai, Tamil Nadu, India
Received: 14/05/2024, Accepted: 10/06/2024, Available online: 12/06/2024
*to whom all correspondence should be addressed: e-mail: ssunil@mitindia.edu
https://doi.org/10.30955/gnj.006173

Graphical abstract

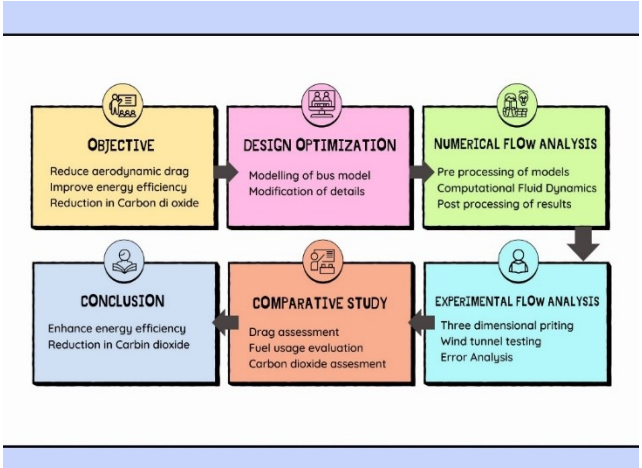

Abstract

Exhaustion of fossil fuel resources, inconsistent fuel costs and the difficulty of adopting electric vehicle technology in commercial vehicles support the idea that there is an opportunity for research in public transit regarding the correlation between energy efficiency and aerodynamic drag. The turbulent external airflow over a bus at high speeds impacts acceleration, speed, and fuel economy. The fundamental bus's design is intended to carry enough passengers for a reasonable run. Envisaging the factors influencing aerodynamic drag is defiant due to the convoluted relationship between the moving bus and the air. Consequently, a comprehensive numerical and experimental exploration is executed on the bodywork of a bus to improve its aerodynamic efficiency (Anwar *et al.* 2021). The aerodynamic drag is directly proportional to the variations in the air density, frontal area, freestream velocity and the drag coefficient. Minimal design reforms are performed on a distinctive long-haul bus. The exertion aims to minimize the drag coefficient, thereby improving the flow characteristics of the bus's bodywork. Through the shape optimization of the bus's bodywork, the modified design has attained a forty-five percent reduction in the drag coefficient. This substantial reduction in drag coefficient directly impacts the reduction of drag force, energy efficiency improvement, and carbon emissions reduction.

Keywords

Aerodynamic drag, Carbon dioxide emissions, Energy efficiency, Steady flow, Three-dimensional printing

1. Introduction

Buses are popularly utilized in commercial conveyance for diverse applications like short and long-haul commuting. Specially designed buses are employed for airport shuttles and mobile showrooms. Long-haul buses are operated at relatively higher average speeds on express motorways than other forms (Palmer and McDonald 1980). The long-haul buses are generally heat-ventilated with a closed passenger zone to evade air turbulence and sustain a comfortable thermal environment. These buses will have an overall length of 12 meters, six tyres, an engine capacity of 6000 cubic centimeters and a laden weight of 20 tonnes. The projected mileage of such a long-haul bus is approximately 5-6 kmpl. The rolling, air, gradient, and acceleration resistance influence the tractive resistance of the bus. Considering the route profile of an express motorway, the influence of gradient and acceleration resistances can be disregarded when evaluating the road load. The laden weight, number of tyres and higher operational speed influence higher rolling resistance on the vehicle than aerodynamic drag. However, during high-speed operation, the magnitude of aerodynamic drag is substantial and requires detailed aerodynamic optimization for improved bus mileage.

From the equation of aerodynamic drag as expressed in Eq. 1,

$$D = \frac{1}{2}\rho_{air} A V_{\infty}^{2} C_{D} \quad (1)$$

The aerodynamic drag (D) is influenced by the atmospheric air density (ρ_{air}), the bus's frontal area (A), the air's and the bus's relative velocity (V_{∞}), and the coefficient of aerodynamic drag (C_D). The opportunity to reduce air density, frontal area, and operational speed is tenacious for a highway bus as each parameter has its functional limitations. Henceforth, the drag coefficient shall be

optimized with the utmost thought to enhance the airflow characteristics around the bus (Carr 1967). From this perspective, significant local origins are recognized on the exterior bodywork of the bus for shape optimization without compromising on other functionalities (Gilhaus 1981).

2. Aerodynamic behaviour of the real bus

2.1. Components of resistances

As seen in Figure 1, the extensive pressure difference between the front and rear ends entices more form drag on the bus. Because of the bus's large external surface, the skin friction confers noticeably to the total drag force. On the other hand, the external flow collapses impulsively at the rear region, provoking an increased form drag and reduced skin friction (Barnard 2010). The rear-view mirrors and the roof-mounted air conditioner have limited interference effects on the outside flow, which results in a modest increase in total drag. The separation of the airflow at the sharp edges of the bus results in the formation of the 3-dimensional vortices. The separation increases induced drag upon the vehicle (Beebe and Mason 1976). Hence, by changing the characteristics relating to shape instead of surface, the total drag force can be reduced to a greater extent.

Figure 1. Pressure contour of the real bus

2.2. Physical model of the bus

A representative 12-meter-long highway bus has opted for an aerodynamic assessment in this exertion. The overall length, width, height, wheelbase, wheel track, ride height, angles of approach and departure are not modified to render the traits of the real bus for aerodynamic valuation. The rear-view mirrors are not considered for aerodynamic evaluation as the shape of the mirrors is not optimized. The global dimensions of the bus are given in Figure 2.

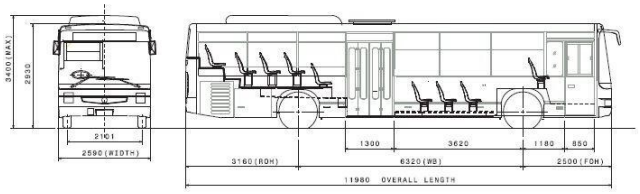

Figure 2. Global dimensions of the real bus

2.3. Generation of finite elements and volumes

The real bus model is disseminated to pre-processing software to generate finite elements over the exterior surface of the bus. As illustrated in Figure 3, about 25,000 finite elements are developed over the bodywork and tyres without any free edges to obtain high precision in the results. Quadrilateral and triangular finite elements are developed over the plane surfaces and curvatures of the bodywork, respectively. Successively, the quality of the lattice is improved by adopting element mending techniques. Consideration has been made to avoid any intersections and overlaps within the elements on the exterior. The lattice quality was maintained at over 99 percent for the evaluations performed.

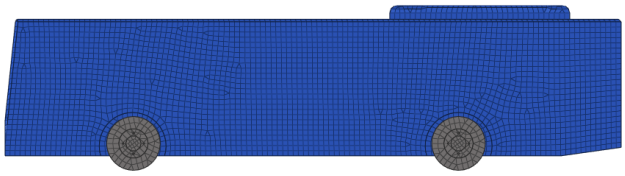

Figure 3. Finite Elements over the bodywork.

2.4. Boundary conditions

The dimensions of a real bus are considered to evaluate the improvement in aerodynamic efficiency, fuel economy and reduction in tailpipe emissions. A wind tunnel is designed virtually to house the pre-processed bus model with finite elements. A rectangular test section is adopted to replicate the tyres on a level road (Jewel *et al.* 1999). As seen in Figure 4, the model is positioned inside the test section, so it has four times its length for upstream airflow and eight times for downstream airflow. The distance between the wind tunnel side walls and the side panels is twelve times the width of the bus. The height of the top wall is fourteen times that of the bus.

Figure 4. Bus model inside a virtual test area.

The ratio between the bus model's projected area and the wind tunnel's cross-sectional area is 0.20%. The pressure outlet is considered at the wind tunnel outlet to achieve reduced velocity at the exit. These boundary conditions are accounted for to replicate the real-time driving scenario. Slip walls are incorporated into the test section's design to stop flow reversal onto the model. However, the test section's floor, the model's outer panels, and the wheels have non-slip surfaces to support the development of the boundary layer. A steady airflow analysis is considered for validation as the bus will not be subjected to frequent acceleration and braking on highways. The mean speed of a typical long-haul bus on a highway is 72 kmph, which, rather than the top speed, is taken into account for the flow analysis. As the values began to get saturated at the 150th step, a 300-number time step was supposed to converge the findings. The Large Eddy Simulation (LES) method involves extensive computational time. Hence, the Reynolds-Averaged Navier-Stokes (RANS) based Spalart–Allmaras turbulence model is carefully chosen, considering its dependability towards findings for external aerodynamic applications. As shown in Figure 5, three refinement zones with 15 lakh finite volumes are created

around the bus model to obtain precise results for flow analysis. Fourteen observing probes are mounted across the external bodywork to measure the magnitudes of essential parameters, including pressure and velocity. Following the simulated flow analysis, the C_D of the real bus is estimated to be 0.84.

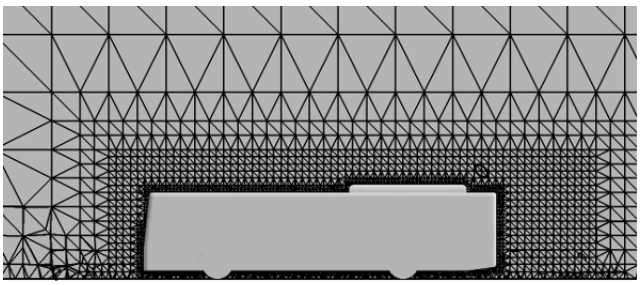

Figure 5. Finite volumes with three distinctive refinement zones

3. Design optimization

Four prime zones are sensibly selected from the external flow phenomena of the real bus model for design transformation. This methodology does not change the significant parameters, such as overall length, maximum width, and height above the ground. However, the details' radius, distance, position, and angle are changed to reach an ideal point without impacting the bus's essential functionality. The blend of ideal changes from the four zones is further integrated into the reformed bus to appraise the improvement in aerodynamic efficiency.

3.1. Frontal region

The slowdown of the air at the windshield influences the splitting of streamlines and their reconnecting downstream upon the roof and side panels [11]. Low-pressure zones are present when the air stream splits and reconnects over the forebody of the bus. Therefore, the windshield angle δ determines the prospect of reducing the low-pressure zones. The real bus model has a windscreen angle of 6°, which is increased by 3° degrees to 18° without compromising the doorway's position or the driver's view, as shown in Figure 6. A flow analysis of a sharp edge design is performed to assess the flow characteristics at the roof front edge. With an edge radius R_1 of 5 cm for the real bus, it is observed that compared to the real bus, the flow separation is more noticeable near the sharp edge. With this realization, to assess R1's relationship to C_D, it was raised to 30 cm at intervals of 5 cm, as shown in Figure 7.

Further increase in R_1 will reduce aerodynamic drag and hence not be considered since it would lead to a major divergence from the front-end design, which would not be used in buses intended for production. The bus front and rear pillars are remarkable structures strengthen the bus framework. There is also three-dimensional lateral external flow separation over the bus body. The splitting of airflow adjacent to the front pillars reconnects alongside the side bodywork. Increasing the curvature R_2 of the front pillars is done to enhance the flow quality at the front lateral ends. The real bus model's R_2 is 5 cm, which was raised to 30 cm at intervals of 5 cm, as shown in Figure 8. A further increase in R_2 will increase the blind spot area and necessitate specific reinforcements in the lateral directions, which is not considered. So as to adopt the optimizations mentioned above upon the windscreen, roof front edge, and front pillars, it is perceived that the attached flow characteristics across the frontal region improve substantially, as comprehended by the reduction in the C_D of 32%.

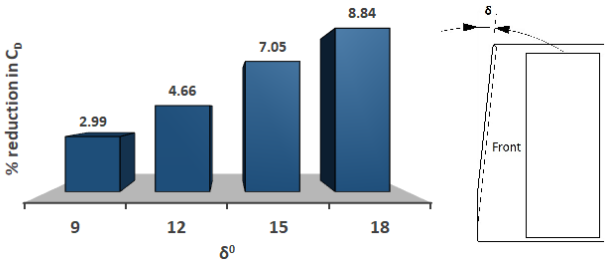

Figure 6. Windscreen angle, δ vs % reduction in CD

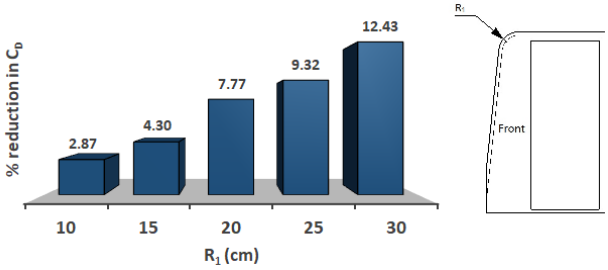

Figure 7. Roof front edge, R1 vs % reduction in CD

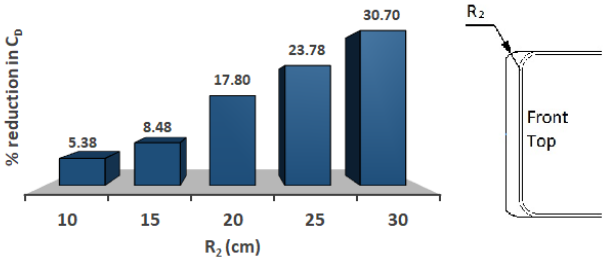

Figure 8. Front Pillar thickness, R_2 vs % reduction in C_D

3.2. Rear region

The rear end has a slant angle of ψ between 0° and 3° for better visual appeal and structural rigidity. The bus's blunt rear end causes the exterior flow over the roof and side panels to suddenly disperse into the environment, which leads to a highly turbulent flow in the posterior region. The dispersed outward flow reattaches at a farther distance from the bus. Smooth paneling and a shorter reattachment distance from the bus's rear end will induce reduced drag. Hence, the ψ is varied up to 18° with an increment of 3° to evaluate the change in C_D, as shown in Figure 9. An additional increase in ψ will reduce the rear passenger area and hence not considered as no further drag reduction is noticed.

Like the front roof edge, an analysis of a sharp roof edge design R_3 is executed to assess the flow characteristics at the rear roof edge. The results reveal that the airflow separation at the sharp rear edge is higher than the real bus with the edge radius R_3 of 5 cm. Consequently, R_3 is improved to 30 cm with a raise of 5 cm to assess its outcome with C_D, as shown in Figure 10. The reduction in C_D is less pronounced by increasing R_3 beyond 20 cm and hence ignored. The edge curvature R_4 of the rear pillars

usually is 5 cm. The airflow on the front windows and side panels separates rapidly at the rear region, instigating high turbulence. This results from the airstream being reattached farther from the bus's rear end. The induced drag of the vehicle is directly proportional to the volume of the low-pressure zone at the rear region. Hence, the edge curvature R_4 of the rear pillars is varied to 30 cm with a 5 cm increment to shrink the low-pressure region at the rear, as shown in Figure 11. Nor is the visibility of the driver or rear row passenger space affected by this optimization. The requirement of the rear diffuser design β enables the bus to navigate gradients and houses the extra wheel. Ideally, the underbody is assumed to be flat with smooth paneling. The external flow from the ground stream smoothly reattaches with the rear external flow at a closer range with the rise in β. Hence, β is increased from 8° to 24° with an increment of 4° to study the effect of change with C_D without affecting the rear occupant and luggage space, as shown in Figure 12. The design optimizations performed at the rear region of the bus yielded a trivial reduction in C_D of 8% yet considered for the modified bus.

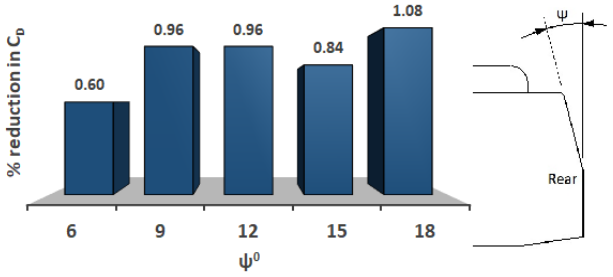

Figure 9. Slant angle, ψ vs % reduction in CD

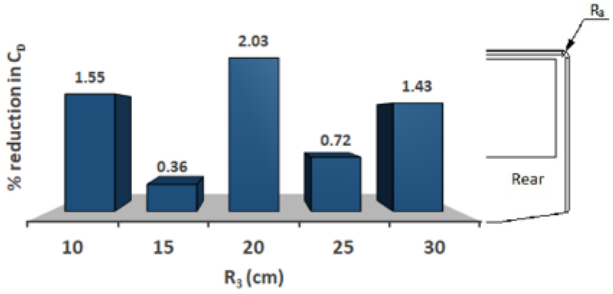

Figure 10. Roof rear edge, R3 vs % reduction in CD

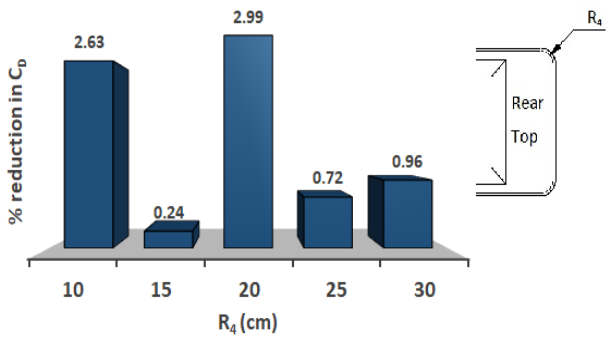

Figure 11. Rear pillar thickness, R4 vs % reduction in CD

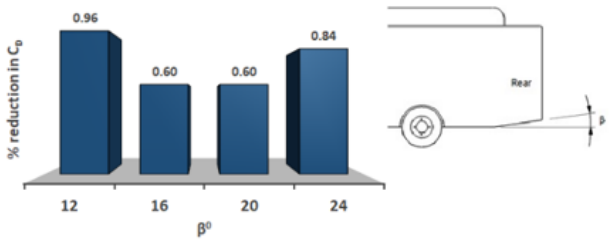

Figure 12. Diffuser angle, β vs % reduction in CD

3.3. Roof and position of air conditioning unit

Typically, the bus's roof paneling is made flat to make room for air conditioners and luggage. Modern bus design provides adequate space to accommodate the baggage beneath the passenger compartment. Three different roof curvature designs, R_5, are incorporated to enhance attached flow characteristics over the roof, as shown in Figure 13. The roof panels are designated with curvatures along the longitudinal and lateral directions to enable smooth airflow and crosswind stability over the body surface. A fair reduction of 6% of C_D is noticed in adding curvatures. The increase in the front area and local flow separation is unavoidable at the roof as the air conditioning unit can't be installed in other regions due to practical constraints. The unit's profile is not altered, but the location is varied at four positions on the bus's roof, as shown in Figure 14. The unit's position on the real bus is three-fourths from the front. Iterations are performed by relocating the unit to the extreme front, extreme rear, centre and one-fourth from the front end. The unit's position at the forefront of the roof boosts drag since the airflow cannot be reattached from the windscreen effectively. The turbulence at the back region increases when the unit is positioned at the roof's rear end due to separated airflow at the rear. The abovementioned positions raised pressure drag close to the unit and hence avoided. The position of the unit at the centre and one-fourth from the front end induces a reduced C_D. The position of the unit, one-fourth from the front end, offered a noticeable C_D reduction and hence was considered for modification. A minor decrease in the C_D of 7% is observed by optimizing the position of the air conditioning unit.

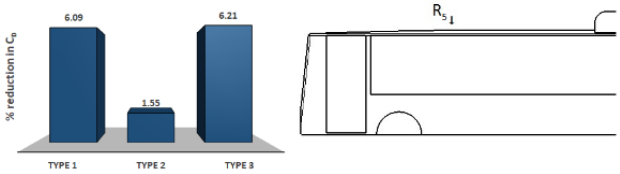

Figure 13. Roof Panels curvatures, R5 vs % reduction in CD

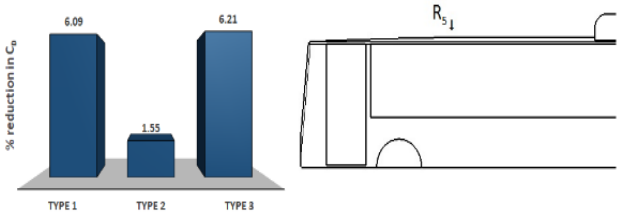

Figure 14. AC position on roof vs % reduction in CD

3.4. Side panels and underbody

For ease of production, the bus side panelling is made straight. The straight side panelling improves the attached flow characteristics during headwinds, as shown in Figure 15. The crosswind sensitivity is efficiently reduced by adopting curved side panels R_6 during side winds. Three distinctive side panel curvatures, R_6, are designed with this in view. The side panels are designated with curvatures along the longitudinal and lateral directions to enrich airflow features and crosswind stability over the body surface. The bus undercarriage is presumed to be flat and composed of smooth panelling. By adopting these optimization strategies into R_6, a significant reduction in C_D of 12% is observed.

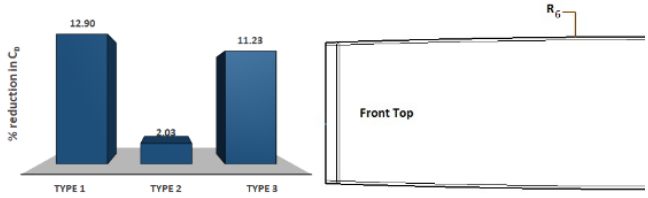

Figure 15. Side Panels curvatures, R6 vs % reduction in CD

4. The optimized bus

During the design optimization, the exterior dimensions of the bus were not modified, as seen in Figure 16.

Figure 16. Comparison of exterior dimensions

The modifications stated above for the real bus are amalgamated for design optimization. The enrichment in the airflow characteristics between the real and modified designs is perceived from the velocity streamlines on the body surface, as illustrated in Figure 17.

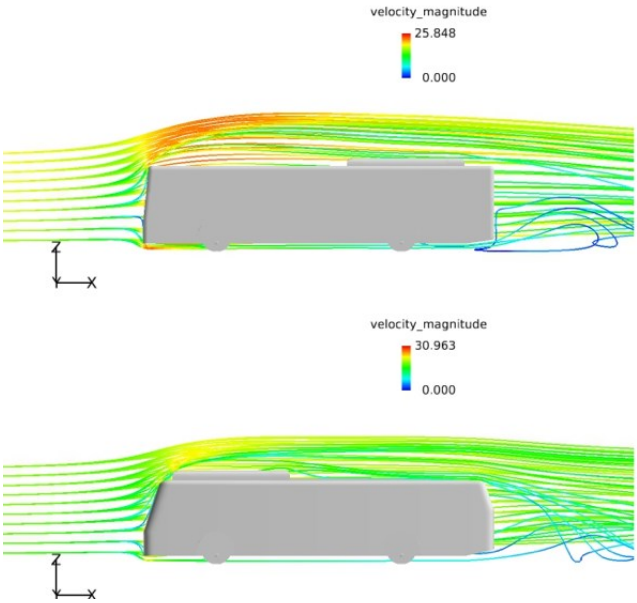

Figure 17. Comparison of velocity streamlines in m/s

A substantial reduction of 45 % C_D is attained in this numerical analysis, resulting in an equivalent decrease in aerodynamic drag.

5. Experimental analysis

The bus models were scaled down and fabricated using a three-dimensional printing technique, as shown in Figure 18.

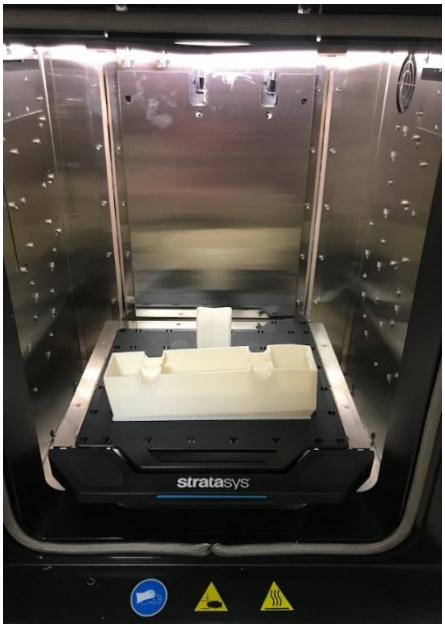

Figure 18. Fabrication of model by three-dimensional printing technique

In order to perform the experimental analysis, a suitable low-speed wind tunnel is selected (Backiyaraj *et al.* 2022). The height and width of the wind tunnel's test area are 0.6 m and 0.6 m, respectively. The bus model is scaled down to a ratio of 1:47 to accommodate it inside the test section effectively, as revealed in Figure 19. The pressure coefficients (C_P) are obtained from significant regions along the longitudinal plane to appraise the airflow around the bus, as shown in Figure 20.

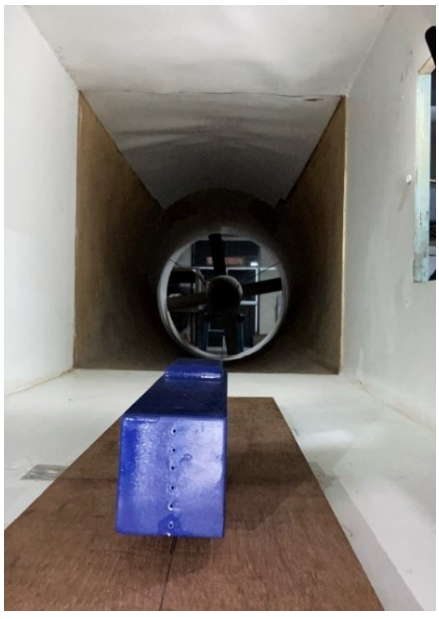

Figure 19. Position of the model inside the wind tunnel

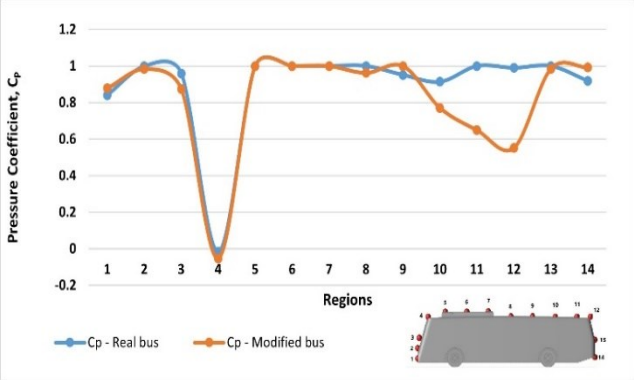

Figure 20. Pressure coefficients CP along the longitudinal plane

From Eq.2,

$$BR = \frac{Projected\ area\ of\ model}{Cross\ sectional\ area\ of\ test\ section} \quad (2)$$

the blockage ratio (BR) was evaluated as less than 2%, ensuring a proper flow characteristic during the analysis. Pressure tappings are incorporated along the longitudinal section of the bus models to determine the coefficient of pressure at cardinal locations. With a free stream velocity of 72 kmph, the flow analysis was performed for the real and modified bus models. The analysis was performed five times to ensure the repeatability and accuracy of the results. The pressure values were measured using a pressure scanner, and the aerodynamic drag force was measured using two load cells. Following the experimental flow analysis, the C_D of the real bus model is found to be 0.75, and the percentage reduction in C_D was found to be 40 % between the existing bus and modified bus models, shown in Figure 21.

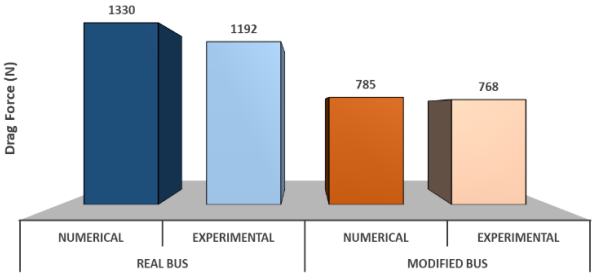

Figure 21. Aerodynamic drag comparison between numerical and experimental analysis

6. Energy efficiency and pollution

6.1. Fuel usage

The ensuing procedure was employed to estimate the fuel usage of the bus models (Cimbala and Cengelo 2013). Aerodynamic drag (D), is evaluated by Eq. 1. considering the functional parameters in Table 1. The energy (*WD*), that has to be utilized for the aerodynamic drag is appraised by Eq. 3.

$$WD = \frac{(D \times x)}{\eta_{eng}} \quad (3)$$

The volume of fuel (V_{fuel}), used to produce (WD) is evaluated by Eq. 4.

$$V_{fuel} = \frac{(WD / CV_{fuel})}{\rho_{fuel}} \quad (4)$$

It is observed that a substantial reduction in fuel consumption of 36 liters per 700 km trip is attained, as shown in Figure 21.

Table 1. Functional parameters

Distance per trip, x	700 km
Energy efficiency of the engine, η_{eng}	30–35%
Calorific value of fuel, CV_{fuel}	42.5 MJ/kg
Fuel density, ρ_{fuel}	850 kg/m^3

6.2. Carbon dioxide reduction

The fuel burns stoichiometrically to produce carbon dioxide (CO_2) and steam (H_2O) as byproducts and a significant amount of heat. Diesel has a density of 850 kg/m^3 and an 86.2% carbon content by composition (Heywood 1988; IPCC 2006). It has been determined that 2.64 kg/m^3 of CO_2 is formed during the complete combustion unit volume of diesel. As shown in Figure 22, the modified design with a drag reduction of 45% will generate 97 kg of CO_2, less than the real bus per trip, endorsing sustainability.

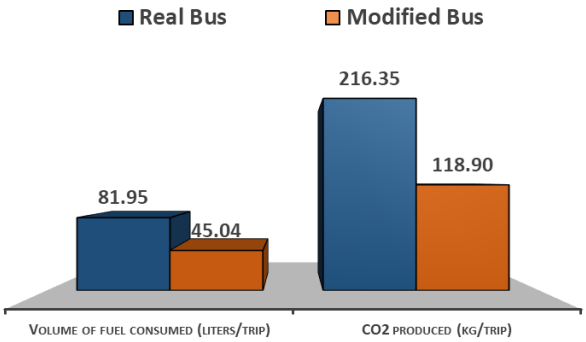

Figure 22. Comparative analysis of fuel usage and CO_2 emissions

7. Conclusion

In the past, advances have been made to drastically reduce the coefficient of drag of a bus below 0.4. Still, they have emphasized revolutionary designs that are difficult to implement for manufacturing. In this effort to improve energy efficiency and reduce carbon emissions, the critical dimensions of the bus were not altered to fulfil the existing norms and ease of production. Crucial regions in the real bus model were optimized to improve the airflow characteristics around the exterior bodywork, which resulted in a 45 % drag reduction. Constructive aerodynamic design optimization has reduced fuel consumption by 36 liters and the equivalent formation of carbon dioxide emission by 97 kg per 700 km trip per bus.

Acknowledgements

The authors would like to express their heartfelt thanks to the Department of Automobile Engineering, Anna University Chennai, Tamilnadu, India, for the technical support, the Department of Aerospace Engineering, Anna University, Chennai, Tamilnadu, India, for the wind tunnel facilities and Centre for Research, Anna University, Chennai, Tamilnadu, India, for the moral support during this exertion.

References

Backiyaraj A., Kumaran T., Parthasarathy M., Murugu Nachippan N. and Senthilkumar P.B. (2022). Vehicle Aerodynamics and Different Testing Methods. (IGI Global) (2022). Barnard R.H., Road Vehicle Aerodynamic Design, 3rd Revised edition. UK: Mechaero Publishing, (2010).

Barlow J.B., Rae W.H. and Pope A. (1999). Low–Speed Wind Tunnel Testing, 3rd edition. John Wiley and Sons.

Beebe P.S. and Mason Jr W.T. (1976). The drag-related flow field characteristics of trucks and buses, Aerodynamic Drag Mechanisms of Bluff Bodies and Road Vehicles. Warren: General Motors Research Laboratories Symposium.

Carr G.W. (1967). The aerodynamics of basic shapes for road vehicles. Part 1: Simple rectangular bodies. Motor Industry Research Association (MIRA).

Cimbala J.M. and Cengel Y.A. (2013). Fluid Mechanics: Fundamentals and Applications, Third Edition. McGraw Hill Education.

Faisal A., Gulavani R.A., Chalipat S., Jadhav S. (2021). Aero Drag Improvement Study on Large Commercial Vehicles Using CFD Lead Approach Aerodynamic drag reduction of intercity buses. (SAE).

Gilhaus A. (1981). The main parameters determining the aerodynamic drag of buses. CSTB Nantes: Proc. of the Colloquium Design with the Wind.

Heywood J. (1988). Internal Combustion Engine Fundamentals. McGraw-Hill.

IPCC. (2006). Guidelines for National Greenhouse Gas Inventories, 2 (Energy). Geneva, Switzerland: *Intergovernmental Panel on Climate Change*.

Lajos T., Preszler L. and Finta L. (1988). Styling and aerodynamics of buses. (*International Journal for Vehicle Design*).

Palmer G.M. and McDonald A.T. (1980). Aerodynamic drag reduction of intercity buses. (SAE).